

Ribose 2'-O-methylation provides a molecular signature for the distinction of self and non-self mRNA dependent on the RNA sensor Mda5

Article

Accepted Version

Zust, R., Cervantes-Barragan, L., Habjan, M., Maier, R., Neuman, B. W., Ziebuhr, J., Szretter, K. J., Baker, S. C., Barchet, W., Diamond, M. S., Siddell, S. G., Ludewig, B. and Thiel, V. (2011) Ribose 2'-O-methylation provides a molecular signature for the distinction of self and non-self mRNA dependent on the RNA sensor Mda5. *Nature Immunology*, 12. pp. 137-143. ISSN 1529-2916 doi: 10.1038/ni.1979 Available at <https://centaur.reading.ac.uk/17078/>

It is advisable to refer to the publisher's version if you intend to cite from the work. See [Guidance on citing](#).

To link to this article DOI: <http://dx.doi.org/10.1038/ni.1979>

Publisher: Nature Publishing Group

the [End User Agreement](#).

www.reading.ac.uk/centaur

CentAUR

Central Archive at the University of Reading

Reading's research outputs online

Ribose 2'-O-methylation provides a molecular signature for MDA5-dependent distinction of self and non-self mRNA

4 Roland Züst^{1#}, Luisa Cervantes-Barragan^{1#}, Matthias Habjan¹, Reinhard Maier¹, Benjamin W.
5 Neuman², John Ziebuhr^{3,4}, Kristy J. Szretter⁵, Susan C. Baker⁶, Winfried Barchet⁷, Michael S.
6 Diamond⁵, Stuart G. Siddell⁸, Burkhard Ludewig^{1,9} and Volker Thiel^{1,9*}

¹Institute of Immunobiology, Kantonal Hospital St. Gallen, St. Gallen, Switzerland. ²School of Biological Sciences, University of Reading, United Kingdom. ³Centre for Infection and Immunity, Queen's University Belfast, Belfast United Kingdom. ⁴Institute of Medical Virology, Justus Liebig University Giessen, Giessen, Germany. ⁵Departments of Medicine, Molecular Microbiology, and Pathology & Immunology, Washington University School of Medicine, St Louis, MO 63110, USA. ⁶Department of Microbiology and Immunology, Loyola University Stritch School of Medicine, Maywood, Illinois, USA. ⁷Institute for Clinical Chemistry and Pharmacology, University Hospital, University of Bonn, Germany ⁸Department of Cellular and Molecular Medicine, School of Medical and Veterinary Sciences, University of Bristol, Bristol, United Kingdom. ⁹Vetsuisse Faculty, University of Zürich, Switzerland.

Running Title: Evasion of innate immune sensing by viral RNA 2'-*O*-methylation

Key words: Interferon, MDA5, coronavirus, RNA methylation, 2'-O-methyltransferase

*Corresponding author:

Volker Thiel; Kantonal Hospital St.Gallen, Institute of Immunobiology, 9007 St.Gallen, Switzerland.

Phone: +41-71-4942843; fax: +41-71-4946321; e-mail: volker.thiel@kssg.ch

R.Z. and L.C-B contributed equally to this work.

28 **ABSTRACT**

29 The 5'-cap-structures of higher eukaryote mRNAs are ribose 2'-*O*-methylated. Likewise, a
30 number of viruses replicating in the cytoplasm of eukaryotes have evolved 2'-*O*-
31 methyltransferases to modify autonomously their mRNAs. However, a defined biological role of
32 mRNA 2'-*O*-methylation remains elusive. Here we show that viral mRNA 2'-*O*-methylation is
33 critically involved in subversion of type-I-interferon (IFN-I) induction. We demonstrate that
34 human and murine coronavirus 2'-*O*-methyltransferase mutants induce increased IFN-I
35 expression, and are highly IFN-I sensitive. Importantly, IFN-I induction by 2'-*O*-
36 methyltransferase-deficient viruses is dependent on the cytoplasmic RNA sensor melanoma
37 differentiation-associated gene 5 (MDA5). This link between MDA5-mediated sensing of viral
38 RNA and mRNA 2'-*O*-methylation suggests that RNA modifications, such as 2'-*O*-methylation,
39 provide a molecular signature for the discrimination of self and non-self mRNA.

40

41

42 **INTRODUCTION**

43 Innate immune recognition of pathogen-associated molecular patterns (PAMPs) facilitates
44 the distinction between immunological self and non-self¹. In the case of cytoplasmic viral RNA,
45 this involves detection by cytoplasmic RIG-I-like receptors (RLRs), such as retinoic acid-
46 inducible gene-I (RIG-I) and MDA5. RLR activation results in the initiation of signaling
47 cascades that induce the expression of cytokines, including IFN-I. These interferons, mainly
48 IFN- α and IFN- β , are secreted and can then bind to the IFN-I receptor (IFNAR) and thus
49 transmit a danger signal to neighboring cells. The activated IFNAR triggers the JAK-STAT
50 signaling pathway, inducing the expression of a large array of IFN-stimulated genes (ISGs) with
51 antiviral activity, thus establishing the so-called host cell antiviral state²⁻⁴. These ISGs include
52 the protein kinase PKR, and stress-inducible proteins, such as interferon-induced protein with
53 tetratricopeptide repeats (IFIT) 1 and IFIT2 (also known as ISG56 and ISG54, respectively),
54 which impair the host cell protein synthesis apparatus⁴⁻⁷.

55 Although the distinction between self and non-self RNA is believed to rely on the
56 molecular signatures found in PAMPs, the exact nature of such signatures remains elusive. Both
57 of the cytosolic RLRs, RIG-I and MDA5, have been shown to bind to double-stranded (ds) RNA
58 with the difference that RIG-I appears to prefer short dsRNA, whereas MDA5 can specifically
59 bind long dsRNA⁸. In addition, the 5'-end of RNAs is currently receiving increased attention, as
60 it has been shown that RIG-I can specifically recognize 5'-triphosphate groups on single-stranded
61 and (partially) dsRNAs⁹⁻¹¹. In contrast, eukaryotic mRNAs, which are not recognized by RIG-I
62 or MDA5, usually have a 5'-cap structure that is methylated at the N-7 position of the capping
63 guanosine residue (cap 0), the ribose-2'-*O* position of the 5'-penultimate residue (cap 1) and
64 sometimes at adjoining residues (cap 2)¹². There are two evolutionary forces proposed to be
65 responsible for the presence of 5'-cap structures on eukaryotic mRNAs, namely the appearance
66 of 5'-exonucleases in eukaryotes, and as means of directing mRNA to the eukaryotic ribosome¹³.

67 Thus, eukaryotic mRNA 5'-cap structures are known to increase mRNA stability and
68 translational efficacy. Notably, although N7-methylation has been implicated to be important in
69 many mRNA-related processes, such as transcriptional elongation, polyadenylation, splicing,
70 nuclear export, and efficient translation, there is no obvious indication why higher eukaryotes
71 have evolved mRNA ribose-2'-*O*-methylation in cap 1 and cap 2 structures.

72 The functional significance of mRNA 5'-structures is best illustrated by the fact that many
73 viruses that replicate in the cytoplasm have evolved either alternative 5'-elements, such as small
74 viral proteins linked to the 5'-end of genomic RNA¹⁴, or encode functions associated with 5'-cap
75 formation that are homologous to those found in eukaryotic cells, such as RNA 5'-
76 triphosphatase, RNA guanylyltransferase, RNA guanine-N7-methyltransferase (N7-MTase), and
77 2'-*O*-MTase (e.g. flaviviruses, coronaviruses and poxviruses) (**Fig 1, Supplementary Table 1**).

78 In addition to the well-established role of mRNA 5'-structures in translation, the discovery that
79 RNA 5'-triphosphate groups activate RIG-I^{9,10} suggests that viruses have to hide or modify their
80 RNA 5'-structures to evade innate immune recognition. Interestingly, RIG-I activation is
81 diminished when 5'-triphosphate RNA contains modified nucleotides⁹. Thus, we hypothesize that
82 RNA modifications, such as methylation, could be a critical factor for the activation of RNA-
83 specific pattern recognition receptors (PRRs). Notably, this concept of methylation-based
84 distinction of self and non-self nucleic acids is well-established for DNA, since the methylation
85 status of CpG motifs in DNA is the structural basis of toll-like receptor (TLR) 9 activation¹⁵.
86 Moreover, DNA methylation has long been recognized as the basis for the ancient bacterial
87 restriction and modification systems that allow bacteria to distinguish between foreign DNA and
88 the bacterial genome.

89 Here, we show that viral mRNA 2'-*O*-methylation is biologically significant in the context
90 of host cell innate immune responses. We demonstrate that human and murine coronavirus
91 mutants lacking 2'-*O*-MTase activity induce increased IFN-I expression and are extremely

92 sensitive to IFN-I treatment. Furthermore, we show that a murine coronavirus mutant with an
93 inactivated 2'-*O*-MTase is attenuated in wild type (WT) macrophages but replicates efficiently in
94 the absence of IFN-I receptor or MDA5. Consonantly, coronavirus 2'-*O*-MTase mutants are
95 apathogenic in WT mice but virus replication and spread is restored in mice lacking the IFN-I
96 receptor and in mice lacking the two major sensors of coronaviral RNA, TLR7 and MDA5.
97 Collectively, our results reveal a link between MDA5-mediated sensing of viral RNA and
98 mRNA 2'-*O*-methylation, and suggest that RNA modifications, such as 2'-*O*-methylation,
99 provide a molecular signature for the distinction of self and non-self mRNA.

100

101

102 **RESULTS**103 **Effects of 2'-O-MTase-deficiency in human coronavirus infection**

104 To address the biological significance of mRNA 2'-O-methylation in the context of host
105 cell innate immune responses, we first used a human model of coronavirus infection.
106 Coronaviruses are single-strand (+) RNA viruses, that replicate in the cytoplasm, and have
107 evolved N-7 and 2'-O-MTases to methylate their viral mRNA 5'-cap structures¹⁶⁻¹⁹. The 2'-O-
108 MTase activity is associated with the viral non-structural protein (nsp) 16, which is highly
109 conserved amongst coronaviruses (**Fig. 1a,b**) and an integral subunit of the viral replicase-
110 transcriptase complexes located at virus-induced double membrane vesicles (DMVs) in the host
111 cell cytoplasm. We have generated a recombinant *human coronavirus* strain 229E (HCoV-229E)
112 mutant encoding an inactivated 2'-O-MTase. This mutant, HCoV-D129A, was produced by
113 substituting nsp16 residue D129 of the highly conserved catalytic K-D-K-E tetrad with alanine
114 (**Fig 1b**). Importantly, this substitution has been shown to completely abrogate 2'-O-MTase
115 activity of recombinant, bacterial-expressed feline coronavirus and SARS coronavirus nsp16
116 proteins^{16,18}. The mutant virus displayed a small plaque phenotype, and reduced replication in the
117 human fibroblast MRC-5 cell line (**Fig 2a,b**). Moreover, we could readily 2'-O-methylate
118 poly(A)-containing RNA obtained from HCoV-D129A-infected cells using the vaccinia virus 2'-
119 O-MTase VP39²⁰ *in vitro* (**Fig 2c**), confirming the loss of 2'-O-MTase activity. In contrast, *in*
120 *vitro* 2'-O-methylation of poly(A)-containing RNA derived from HCoV-229E-infected cells was
121 indistinguishable compared to poly(A)-containing RNA obtained from mock infected cells.
122 Importantly, compared to HCoV-229E, we observed significantly increased IFN- β expression in
123 blood-derived human macrophages (M Φ s) following HCoV-D129A infection (**Fig 2d**), and
124 complete restriction of HCoV-D129A replication in human M Φ that had been pretreated with
125 IFN- α (**Fig 2e**). These results suggest a biological role of mRNA 2'-O-methylation in the context
126 of (i) IFN-I induction, and (ii) IFN-I stimulated antiviral effector mechanisms.

127

128 **IFN-I induction by 2'-O-MTase mutants is MDA5-dependent**

129 To extend our studies on the impact of 2'-O-methylation on coronavirus-induced innate
130 immune responses, we used an animal model of coronavirus infection with *mouse hepatitis virus*
131 strain A59 (MHV-A59) as a natural mouse pathogen. Studies on innate immune responses
132 following MHV-A59 infection have shown that plasmacytoid dendritic cells (pDCs) have a
133 unique and crucial role in sensing coronaviral RNA via TLR7, ensuring a swift production of
134 IFN-I following virus encounter^{21,22}. Other target cells, such as primary fibroblasts, neurons,
135 astrocytes, hepatocytes, and conventional dendritic cells, do not produce detectable IFN-I upon
136 MHV infection^{22,23}. The exceptions are MΦs and microglia, which can respond with IFN-I
137 expression upon MHV infection, although only to moderate levels^{24,25}. Importantly however,
138 IFN-I expression detected in MΦs and microglia is dependent on MDA5²⁴.

139 We have generated a recombinant MHV lacking 2'-O-MTase activity by substituting the
140 nsp16 2'-O-MTase active site residue D130 with alanine (MHV-D130A; **Fig 1b**). In addition, we
141 generated a recombinant MHV mutant, designated MHV-Y15A, encoding a Y15A substitution
142 at the putative type 0 cap binding site of nsp16 (**Fig 1b**). This substitution was shown to impair
143 type 0 cap-binding for the corresponding feline coronavirus nsp16 mutant Y14A¹⁸, and we
144 expected that this substitution would reduce, rather than completely abrogate coronaviral mRNA
145 2'-O-methylation. Indeed, the *in vitro* methylation of mRNA with the vaccinia virus 2'-O-MTase
146 VP39²⁰ confirmed the differential 2'-O-methylation of mRNA obtained from MHV-infected
147 cells. As shown in **Figure 3a**, right panel, transfer of [³H]-labeled methyl groups from the
148 methyl donor S-adenosyl-methionine (SAM) to mRNA derived from MHV-Y15A-infected cells
149 was less efficient compared to MHV-D130A mRNA, but significantly increased compared to
150 MHV-A59 mRNA. These results show the loss of 2'-O-MTase activity of MHV-D130A, and
151 that a significant proportion of MHV-Y15A mRNA is not methylated at the 2'-O position.

152 The analysis of virus growth in cell culture revealed that the replication kinetics of both
153 recombinant viruses, MHV-D130A and MHV-Y15A, differed only slightly from those of MHV-
154 A59 following infection of a murine fibroblast 17Cl-1 cell line with high and low multiplicities
155 of infection (MOI; MOI=1 and MOI=0.0001, respectively) (**Fig 3b**). Also, there was no
156 significant difference observed in electron microscope analyses of DMV formation and
157 morphology in the cytoplasm of MHV-A59-, MHV-D130A-, and MHVY15A-infected cells
158 (**Supplementary Fig 1**), which is relevant in relation to cytoplasmic viral RNA sensing, since
159 coronavirus DMVs are known to harbor dsRNA. When we analyzed IFN-I in supernatants of
160 WT MΦs at 15 hours p.i., we observed that infection with both 2'-*O*-MTase mutants, MHV-
161 Y15A and MHV-D130A, resulted in increased IFN-I production (**Fig 3c, Supplementary Fig**
162 **2a**). Likewise, IFN-I was efficiently produced in MHV-D130A and MHV-Y15A infected
163 IFNAR-deficient MΦs compared to MHV-A59 infection, demonstrating that increased IFN-I
164 production by MHV 2'-*O*-MTase mutants is detectable in the absence of IFNAR signaling (**Fig**
165 **3d, Supplementary Figure 2b**). Importantly, in MDA5-deficient MΦs neither MHV-A59, nor
166 the two 2'-*O*-MTase mutant viruses induced any detectable expression of IFN-I (**Fig 3e**),
167 whereas IFN-I production was readily detectable in MDA5-deficient cells following Sendai virus
168 infection. Detailed analysis of IFN-β mRNA expression kinetics revealed that infection of WT
169 (**Fig 3f**) and IFNAR-deficient (**Fig 3g**) MΦs with both MHV-D130A and MHV-Y15A resulted
170 in increased IFN-β gene expression with a peak at 12 h p.i.. Notably, IFN-β induction was most
171 pronounced after infection with the 2'-*O*-MTase active site mutant MHV-D130A. These results
172 indicate that the level of IFN-β expression correlates with the degree of 2'-*O*-methylation
173 deficiency of viral RNA and, that IFN-β induction following infection with 2'-*O*-MTase mutant
174 viruses is MDA5-dependent. Consonantly, we observed increased nuclear localization of
175 interferon regulatory factor 3 (IRF3; a transcription factor that is activated in the RLR signaling

176 pathway and is translocated from the host cell cytoplasm to the nucleus to mediate IFN-I
177 transcription) in MHV-D130A- and MHV-Y15A-infected IFNAR-deficient MΦs, but not in
178 MDA5-deficient MΦs (**Fig 4**). Collectively, these results demonstrate a linkage of mRNA 2'-*O*-
179 methylation and MDA5-dependent induction of IFN- β expression.

180

181 **2'-*O*-methylation affects two distinct antiviral mechanisms**

182 Since the 2'-*O*-MTase active site mutant HCoV-D129A displayed an elevated sensitivity to
183 IFN-I treatment, we assessed whether IFN-I induced restriction of viral replication is also
184 effective against the MHV 2'-*O*-MTase mutants. Therefore, we investigated in more detail the
185 viral replication kinetics of MHV-D130A and MHV-Y15A in primary MΦs, which represent the
186 most important target cells for MHV^{21,26}. MHV-D130A replication was greatly impaired in WT
187 MΦs (even after infection with high MOI; MOI=1), whereas replication of MHV-Y15A was
188 similar to that of MHV-A59 (**Fig 5a**). Importantly, MHV-D130A replication was fully restored
189 in MDA5-deficient MΦs, even after infection with low MOI (MOI=0.0001) (**Fig 5b**). This
190 demonstrates that MDA5-dependent IFN-I expression is a prerequisite for the induction of
191 effective restriction of MHV-D130A replication. In agreement with the notion that the
192 replication of MHV-D130A, but not MHV-Y15A, was impaired in WT MΦs, we observed a
193 remarkable reduction of MHV-D130A replication in WT MΦs that were pretreated with IFN- α .
194 Thus, compared to MHV-A59, MHV-D130A replication was not detectable at 24 h p.i. (after 4 h
195 pretreatment of WT MΦs with 50 - 200 U IFN- α), whereas MHV-Y15A replication was not
196 significantly restricted (**Fig 5c**). Interestingly, in MDA5-deficient MΦs, pretreatment with at
197 least 200 U IFN- α was required to restrict MHV-D130A replication to non-detectable levels (**Fig**
198 **5d**). This suggests that endogenous MDA5-mediated IFN-I expression additionally impacts on
199 MHV-D130A restriction in WT MΦs. Collectively these analyses depict a clear difference

200 between the phenotypes of MHV-D130A and MHV-Y15A. Inactivation of the MHV 2'-*O*-
201 MTase activity by targeting the active site residue D130 led to increased IFN-I production as
202 well as to pronounced sensitivity to IFN-I pretreatment. In contrast, reduction of viral mRNA 2'-
203 *O*-methylation through targeting of the type 0 cap-binding site residue Y15 was sufficient to
204 induce increased IFN-I production but not to confer increased IFN-I sensitivity. Thus, we
205 conclude that there is, in addition to MDA5-dependent IFN-I induction, a second and distinct
206 antiviral mechanism, which is IFN-I-induced and accounts for the restriction of viral replication
207 during the host cell antiviral state.

208 In this respect, Daffis and colleagues have shown recently that the replication of a West
209 Nile virus (family *Flaviviridae*, genus flavivirus) mutant lacking 2'-*O*-methylation was strongly
210 inhibited by IFIT gene family members²⁷, which are ISGs implicated in translational regulation.
211 To assess whether this molecular mechanism also pertains to coronavirus infection, we assessed
212 the replication kinetics of MHV-A59, MHV-D130A, and MHV-Y15A in primary MΦs derived
213 from WT or *ifit1*^{-/-} mice. Remarkably, MHV-D130A replication was almost completely restored
214 in *ifit1*^{-/-} MΦs (Fig 6), analogous to the restoration of MHV-D130A replication in *mda5*^{-/-} MΦs
215 (Fig 5a,b). Collectively, these findings show that the MDA5-dependent IFN-I induction and the
216 IFIT-1-mediated restriction of viral replication are two distinct antiviral mechanisms that are
217 both based on the distinction of 2'-*O*-methylated and non-methylated mRNAs, but operate at
218 different levels of the host cell antiviral response.

219

220 **Impact of 2'-*O*-MTase-deficiency on innate immune recognition *in vivo***

221 Next, we examined the impact of viral mRNA 2'-*O*-methylation on innate immune
222 recognition and virulence *in vivo* and compared the phenotype of MHV-A59 with those of the
223 MHV 2'-*O*-MTase mutants in C57BL/6 (B6) mice after intraperitoneal (i.p.) infection with 500
224 plaque forming units (p.f.u.) of virus (Fig 7a,b). In contrast to MHV-A59, neither of the MHV

225 2'-*O*-MTase mutants were detectable in spleens or livers of B6 mice at 48 h.p.i., demonstrating
226 the importance of viral mRNA 2'-*O*-methylation for efficient replication and spread in the host.
227 Moreover, both MHV 2'-*O*-MTase mutants could replicate and spread in IFNAR-deficient mice,
228 emphasizing the pivotal role of viral mRNA 2'-*O*-methylation as a countermeasure to the host
229 IFN-I response. Finally, in MDA5-deficient and TLR7-deficient mice, the two known receptors
230 recognizing coronaviral RNA, and consonant with the pronounced sensitivity of the 2'-*O*-MTase
231 active site mutant MHV-D130A to IFN- α pretreatment in M Φ s, MHV-D130A was not
232 detectable in spleens or livers of mice lacking either of the RNA sensors. This suggested that
233 induction of IFN-I expression via TLR7 or MDA5 suffices to completely restrict viral replication
234 and spread when viral mRNA 2'-*O*-methylation is abrogated. Interestingly, the type 0 cap-
235 binding mutant MHV-Y15A was still detectable in the spleens of TLR7-deficient and MDA5-
236 deficient mice, suggesting that robust IFN-I induction by both RNA sensors is required to fully
237 restrict viral replication if the 2'-*O*-MTase activity is reduced rather than abrogated. Importantly,
238 in mice deficient for both receptors, TLR7 and MDA5 (*tlr7*^{-/-}/*mda5*^{-/-}), the replication and spread
239 of both MHV 2'-*O*-MTase mutants was indistinguishable compared to IFNAR-deficient mice.
240 These observations confirm that TLR7 and MDA5 represent the main sensor molecules for
241 recognizing coronaviral RNAs and demonstrate that 2'-*O*-methylation of viral mRNA serves as a
242 mechanism to evade host innate immune recognition of non-self RNA *in vivo*.

243

244

245 **DISCUSSION**

246 The correct functioning of host innate immune responses is based on reliable pathogen
247 detection and is essential in limiting pathogen replication and spread. Here, we demonstrate by
248 using human and murine coronavirus models of infection that mRNA 2'-*O*-methylation provides
249 a molecular signature that has a dual role during interaction with the host innate immune
250 responses. First, mRNA 2'-*O*-methylation protects viral RNA from recognition by MDA5 and
251 thus prevents MDA5-dependent IFN-I production in virus-infected cells. Second, 2'-*O*-
252 methylation of viral mRNA contributes to evasion from the IFIT1-dependent restriction of viral
253 replication that is operative during the IFN-I-induced host cell antiviral state. Moreover, this
254 study shows that these distinct processes can be uncoupled either in the absence of IFN-I
255 signaling (e.g. in IFNAR-deficient cells/mice), or through a genetic approach that targets the
256 cap-0 binding residue Y15 of MHV nsp16. Apparently, the lack of 2'-*O*-methylation on a
257 proportion of MHV-Y15A mRNAs is sufficient to trigger the MDA5 pathway of IFN-I
258 induction, whilst the MHV-Y15A mRNAs that are 2'-*O*-methylated allows the virus to evade the
259 IFIT1-mediated restriction of viral replication. In contrast, the absence of 2'-*O*-methylation of
260 viral RNA through targeting of the 2'-*O*-MTase active site residue D130 strongly activates the
261 MDA5 pathway and results in restriction of virus propagation.

262 The data provided in this study elucidate the impact of mRNA 2'-*O*-methylation on
263 MDA5-dependent induction of IFN-I. The use of human and murine systems of coronavirus
264 infection greatly facilitated the analysis of this link because (i) coronaviruses encode their own 5'
265 mRNA cap methylation machinery, which allowed us to study the phenotype of recombinant
266 viruses with mutated 2'-*O*-MTase proteins, and (ii) the induction of IFN-I expression is hardly
267 detectable in infected cells, other than pDCs, with the notable exception of MΦs, which produce
268 a low level of MDA5-mediated IFN-I following infection^{22-24,28}. In contrast, most other RNA
269 viruses that replicate in the cytoplasm induce considerable levels of IFN-I that may mask the

270 specific impact of mRNA 2'-*O*-methylation on MDA5 activation^{2,29}. In future studies it will be
271 important to clarify whether viral mRNA lacking 2'-*O*-methylation is directly recognized by
272 MDA5, resulting in its activation, or whether it is part of the activation signal of MDA5, possibly
273 in combination with dsRNA regions. The reverse genetic approach used in this study provided
274 evidence for the biological significance of mRNA 2'-*O*-methylation in the context of MDA5-
275 dependent IFN-I induction, and we expect that the generation of further recombinant viruses,
276 harboring defined mutations in RNA-processing enzymes, combined with biochemical
277 approaches will be useful in the identification of naturally occurring MDA5 ligands.

278 The evasion of MDA5-dependent RNA recognition and IFIT gene member dependent
279 restriction of virus replication provide a reasonable explanation for the conservation of 2'-*O*-
280 MTases in many viruses replicating in the cytoplasm of higher eukaryotes (**Supplementary**
281 **Table 1**). It is also striking that a number of viruses, such as bunyaviruses and arenaviruses,
282 which replicate in the cytoplasm but have not acquired the ability to autonomously generate and
283 modify their 5'-cap structures, have evolved means to snatch the cap structure from cellular
284 mRNA^{30,31} (**Supplementary Table 1**). Moreover, structural and functional analyses of the Lassa
285 virus (family *Arenaviridae*) nucleoprotein have revealed that this cap-binding protein can
286 antagonize IFN-I through its associated 3' – 5' exoribonuclease activity, probably by cleaving
287 RNAs that function as PAMPs³². The protein also has an unusually deep cap-binding pocket that
288 has been proposed to accommodate the entire m7GpppN cap structure³². Thus it is potentially
289 able to recognize and discriminate between 2'-*O*-methylated and non-methylated capped RNAs.
290 Finally, members of the *Picornavirales* order and related viruses, which replicate in the
291 cytoplasm but do not encode MTases, have evolved alternative 5'-ends of their viral RNAs.
292 These viruses covalently attach a small viral protein (VPg) to the genomic 5'-terminus and
293 harbor an internal ribosomal entry site at the 5'-non-translated region³³ (**Supplementary Table**
294 **1**). Interestingly, encephalomyocarditis virus (EMCV, family *Picornaviridae*) replication appears

295 not to be restricted by IFIT proteins²⁷, however, EMCV infection is sensed through the MDA5
296 pathway³⁴. Thus, it is tempting to speculate, that the use of internal ribosomal entry allows
297 EMCV to evade host restriction by IFIT family members, but the covalent attachment of VPg to
298 picornaviral RNA 5'-termini does not prevent MDA5-dependent RNA recognition and IFN-I
299 induction.

300 A relationship between RNA modification and host cell innate immune responses is further
301 supported by observations made during studies of cellular PRRs. For example, it has been shown
302 that activation of RIG-I and PKR is diminished when 5' triphosphate RNA contains modified
303 nucleotides^{9,10,35}. Similarly, nucleoside modifications reduce the potential of RNA to trigger
304 TLRs³⁶. Although, most of these observations have been made by in vitro studies (e.g. the
305 transfection of short synthetic RNAs), it appears that RNA modifications may impact on innate
306 immune sensing on a wider scale³⁷. Therefore, it will be important to extend our knowledge on
307 naturally occurring RNA modifications and their impact on innate immune responses. We
308 predict that the analysis of viral RNA modifications will most likely unveil further molecular
309 RNA signatures that function as PAMPs.

310 In summary, our study identifies 2'-*O*-methylation of eukaryotic mRNA cap structures as a
311 molecular pattern of self mRNAs, and demonstrates that there are at least two cellular
312 mechanisms that allow for the distinction of 2'-*O*-methylated versus non-methylated mRNAs.
313 Consequently, a number of viruses replicating in the cytoplasm, without access to the nuclear
314 host cell mRNA capping and modification machinery, have evolved to encode their own RNA-
315 modifying enzymes as means of mimicking cellular mRNAs. Our data should encourage future
316 studies to evaluate the full spectrum and functional significance of mRNA modifications as an
317 additional layer of information imprinted on eukaryotic mRNAs.

318

319 **METHODS SUMMARY**

320 **Mice, viruses, cells and virus infection.** C57BL/6 mice were obtained from Charles River
321 Laboratories (Sulzfeld, Germany). *ifnar*^{-/-}, *mda5*^{-/-}, *tlr7*^{-/-}, and *mda5*^{-/-} × *tlr7*^{-/-} mice were on the
322 C57BL/6 background and bred in the animal facilities of the Kantonal Hospital St.Gallen. *ifit1*^{-/-}
323 mice were bred in the animal facilities of the Washington University School of Medicine. All
324 mice were maintained in individually ventilated cages and were used between 6 and 9 weeks of
325 age. All animal experiments were done in accordance with the Swiss Federal legislation on
326 animal protection and the Saint Louis University Animal Studies Committees.

327 HCoV strain 229E, HCoV-D129A, MHV strain A59, MHV-D130A and MHV-Y15A
328 recombinant viruses were generated using a vaccinia virus-based reverse genetic system as
329 described³⁸ and propagated on either Huh-7 (HCoV) or 17Cl1 (MHV) cells. BHK-21, L929,
330 NIH-3T3, Huh-7, MRC-5 and CV-1 cells were purchased from the European Collection of Cell
331 Cultures. D980R cells were a kind gift from G. L. Smith, Imperial College, London, UK. 17Cl1
332 cells were a kind gift from S.G. Sawicki, Medical University of Ohio, Toledo, Ohio, USA.

333 BHK-MHV-N and BHK-HCoV-N cells, expressing the MHV-A59 or HCoV-229E
334 nucleocapsid protein, respectively, under the control of the TET/ON system (Clontech), have
335 been described previously³⁸. All cells were maintained in minimal essential medium
336 supplemented with fetal bovine serum (5-10%) and antibiotics. Thioglycolate-elicited murine
337 macrophages were generated as described³⁹. Human macrophages were isolated from peripheral
338 blood of normal donors as described⁴⁰.

339 Mice were injected intraperitoneally (i.p.) with 500 p.f.u. of MHV. Organs were stored at –
340 70°C until further analysis. Virus infection of human blood-derived macrophages and
341 thioglycolate-elicited murine macrophages was done in a 24-well format with 0.5-1×10⁶ cells
342 and the indicated MOI. MHV titers were determined by standard plaque assay using L929 cells.

343 HCoV titers were determined by plaque assay using Huh-7 cells that were overlaid at 1 h p.i.
344 with 1.2% Avicel/10% DMEM and stained with crystal violet 3 days post infection.

345 **2'-O-methylation of poly(A)-containing RNA *in vitro*.** Poly(A)-containing RNA was
346 isolated using the Dynabeads mRNA DIRECT Kit (Invitrogen, Basel, Switzerland) from 1×10^7
347 mock- or HCoV-infected (MOI=1; at 48 h p.i) Huh-7 cells, and from 1×10^7 mock- or MHV-
348 infected (MOI=1; at 24 h p.i.) NIH-3T3 cells according to the manufacturer's recommendation.
349 The RNA was precipitated after adding 0.1 volume of 4 M ammonium-acetate and 1 volume of
350 isopropanol, washed with 70% ethanol and dissolved in 10 mM TRIS-HCl (pH 7.5) to a final
351 concentration of 150 ng/ μ l. In vitro 2'-O-methylation reactions contained 300 ng of poly(A)-
352 containing RNA derived from virus-infected cells or a corresponding amount of poly(A)-
353 containing RNA from non-infected cells (as determined by qRT-PCR using murine GAPDH and
354 human β -actin specific primers; data not shown) using the ScriptCap 2'-O-Methyltransferase
355 (Epicentre Biotechnologies, Madison, USA) in 0.5 μ M SAM and 1.4 μ M 3 H-labeled SAM (78
356 Ci/mmol; Perkin Elmer, Schwerzenbach, Switzerland) for 1 h at 37°C. Reactions were purified
357 using SigmaSpin Post-Reaction Clean-Up columns (Sigma-Aldrich, Buchs, Switzerland), and
358 the eluates were mixed with 2 ml Ultima Gold scintillation fluid to measure 3 H-incorporation as
359 counts per minute using a Packard Tri-Carb Liquid Scintillation Counter (Perkin Elmer,
360 Schwerzenbach, Switzerland).

361 **Immunofluorescence, IFN- β ELISA and IFN- α pre-treatment.** Detection of IRF3 was
362 done on thioglycolate-elicited murine macrophages (2×10^5 per well in 200 μ l) that were seeded
363 in 8- chamber tissue culture glass slides (BD Falcon), incubated over night at 37°C and infected
364 with MHV at an MOI=1. At 3h p.i. cells were stained for IRF3 (Clone FL-425, Santa Cruz
365 Biotechnology) and DAPI. Images were acquired using a Leica DMRA microscope (Leica,
366 Heerbrugg, Switzerland). Mouse and human IFN- β concentrations in cell culture supernatants

367 was measured by ELISA (PBL Biomedical Laboratories, NJ, USA) according to manufacturers'
368 instructions. IFN- α pre-treatment of cells prior to virus infection was done using universal type I
369 interferon (IFN- α A/D, Sigma, Buchs, Switzerland).

370 **Bioassay for type I interferon (IFN-I).** Total IFN-I in supernatants was measured using
371 LL171 cells (kind gift from M. Pelegrin, Institut de Génétique Moléculaire de Montpellier,
372 France), which are L929 cells stably transfected with a luciferase reporter plasmid under control
373 of the IFN-stimulated response element (ISRE-Luc)⁴¹. Recombinant IFN-A/D (Sigma) was used
374 as a cytokine standard. Prior to measurement, virus was removed by centrifuging supernatants
375 through AMICON spin columns with a cutoff of 100 kDa (Millipore) according to the
376 manufacturer's instructions. LL171 cells grown in 96-well plates were treated with column-
377 filtered supernatants for 6 hours, and luciferase activity was detected upon addition of Bright-
378 Glo Luciferase substrate (Promega) in a GloMax 96 Plate Luminometer (Promega). All
379 measurements were done in duplicate. The sensitivity threshold of the assay was between 5 and
380 15 U/ml IFN.

381 **Quantitative RT-PCR.** Total cellular RNA was isolated with the NucleoSpin RNA II kit
382 (Macherey-Nagel) according to the manufacturer's instructions and used as template for cDNA
383 synthesis using the High Capacity cDNA Reverse Transcription kit (Applied Biosystems). IFN- β
384 and TATA-box binding protein (TBP) mRNA levels were detected with the LightCycler
385 FastStart DNA Master^{PLUS} SYBR Green I kit (Roche) on a LightCycler 1.5 (Roche). The
386 following primers were used: IFN- β 5'-GGTGGAAATGAGACTATTGTTG-3' and 5'-AGGACA
387 TCTCCCACGTC-3', TBP 5'-CCTTCACCAATGACTCCTATGAC-3' and 5'-CAAGTTACA
388 GCCAAGATTAC-3'. Measurements were done in duplicate and relative expression of IFN- β
389 was normalized to the mock data by the comparative cycling threshold method ($\Delta\Delta C_T$).

390 **Phylogenetic analysis of viral MTase domains.** Regions of MTase homology have been
391 identified previously as members of the RrmJ-like superfamily, InterPro IPR002877. Additional

392 members of this protein family were identified by BLAST searches using previously-identified
393 RrmJ-like amino acid sequences using the default search parameters. For virus species
394 belonging to a family in which an RrmJ-like domain had been identified, structure-based amino
395 acid alignment was done to determine whether a distant homolog might be present. We
396 compared predicted and actual secondary structures from confirmed 2'-*O*-MTase domains to
397 secondary structure predictions of domains of unknown function. Secondary structures were
398 predicted using PsiPred version 3.0. Putative secondary structure matches were considered as
399 confirmed upon identification of the best-conserved MTase motifs I, IV, VI, VIII and X⁴².
400 Viruses in which we were unable to identify a primary or secondary structure match to RrmJ-like
401 proteins are marked “not detected” in **Supplementary Table 1**.

402

403 **FIGURE LEGENDS**

404

405 **Figure 1.** Conservation of viral 2'-*O*-MTases. **a)** Schematic representation of the human
406 and murine coronavirus genomes. The conserved replicase gene is depicted together with viral
407 proteinase cleavage sites (arrowheads) that separate nsps 1–16. The nsp16-associated 2'-*O*-
408 MTase is depicted. **b)** Coronavirus nsp16 proteins belonging to the human fibrillarin and *E. coli*
409 RrmJ-like methyltransferase family⁴³ were analyzed by sequence comparison. Sixteen
410 coronavirus nsp16 amino acid sequences, which were 20–90% identical and are representative of
411 alpha-, beta- and gammacoronaviruses were aligned using ClustalW2⁴⁴. Sequence conservation
412 is shown using a color code that indicates the percentage of amino acid identity. Amino acid
413 residues that have been substituted to alanine in previously published biochemical and structural
414 studies^{16,18} are colored according to the observed phenotype of the mutant protein. Amino acid-
415 to-alanine replacements characterized in this and previous studies are depicted. **c)** Conservation
416 of viral and cellular methyltransferase motifs. Alignment of MHV nsp16 with homologous

417 methyltransferases from White bream virus (WBV; order *Nidovirales*), Dengue virus (DENV;
418 family *Flaviviridae*), Vesicular stomatitis virus (VSV; order *Mononegavirales*), Vaccinia virus
419 (VACV; family *Poxviridae*), and human fibrillarin (FBL; *Homo sapiens*) was done using
420 ClustalW2 and manually adjusted based on published structural data and PSIPRED protein
421 secondary structure predictions⁴⁵. Motif nomenclature follows Fauman *et al.*⁴². Coloring reflects
422 amino acid similarity and conservation as implemented in JalView⁴⁶.

423

424 **Figure 2.** The HCoV 2'-*O*-MTase active site mutant has altered replication kinetics, is
425 defective in ribose 2'-*O*-methylation, induces increased levels of IFN- β , and is IFN-I sensitive. **a)**
426 Analysis of plaques produced by HCoV-229E and HCoV-D129A. **b)** HCoV-229E and HCoV-
427 D129A replication kinetics in MRC-5 cells after infection at an MOI=0.1. Results are the
428 average of two independent experiments done in triplicate. **c)** ³H-incorporation (counts per
429 minute; cpm) into poly(A)-containing RNA derived from mock-infected (self RNA), HCoV-
430 229E-, and HCoV-D129A-infected (non-self RNA) cells after *in vitro* 2'-*O*-methylation using the
431 vaccinia virus 2'-*O*-MTase VP39. Results represent the mean \pm SD of three independent
432 experiments. **d)** IFN- β production of human blood-derived M Φ s after infection with HCoV-
433 229E and HCoV-D129A. Cells (1×10^6) were infected at an MOI=1 and 24 h p.i. IFN- β was
434 measured in the culture supernatant by ELISA. Results are plotted for each of the 9 independent
435 donors and data points from individual donors are connected by lines. Mean values (thick bars)
436 \pm SD (thin bars) are indicated and statistical analysis was done using Wilcoxon matched pairs test
437 (**, p < 0.005). **e)** Human blood-derived M Φ s were pretreated with increasing doses of IFN- α 4
438 h prior to infection with HCoV-229E or HCoV-D129A at MOI=1. At 24 h p.i., supernatants
439 were harvested and viral titers were measured by plaque assay. ND: not detected.

440

441 **Figure 3.** MHV 2'-O-MTase mutants induce IFN- β in an MDA5-dependent manner. **a)**
442 Poly(A)-containing RNA (300 ng) from MHV-A59, MHV-Y15A and MHV-D130A infected
443 cells was separated on a standard 1% agarose gel and stained with ethidium-bromide (left panel).
444 Genomic and subgenomic mRNAs (mRNA 1-7) and their respective sizes (in kb) are indicated.
445 The right panel shows 3 H-incorporation (cpm) into poly(A)-containing RNA derived from mock
446 infected (self RNA), MHV-A59-, MHV-Y15A- and MHV-D130A-infected (non-self RNA) cells
447 after *in vitro* 2'-O-methylation using the vaccinia virus 2'-O-MTase VP39. Results represent the
448 mean \pm SD of seven independent experiments. **b)** Replication kinetics of MHV-A59, MHV-
449 Y15A and MHV-D130A in 17Cl1 cells. Cells were infected at an MOI=1 (left panel) or
450 MOI=0.0001 (right panel), and viral titers in cell culture supernatants were determined at the
451 indicated time points p.i.. **c-e)** Murine M Φ s (1×10^6) derived from WT (**c**), *ifnar*^{-/-} (**d**), or *mda5*^{-/-}
452 (**e**) mice were infected at an MOI=1 and IFN- β concentration was determined in cell culture
453 supernatants by ELISA at 15 h p.i.. Results represent the mean \pm SD of three independent
454 experiments (n=6). **f,g)** Quantitative RT-PCR for IFN- β . WT (**f**), or *ifnar*^{-/-} (**g**) M Φ s were
455 infected as described above and IFN- β mRNA expression levels were analyzed by quantitative
456 RT-PCR at the indicated time points. Results represent the mean \pm SD of two independent
457 experiments (n=6). Statistical analysis was done using unpaired Student's t-test (***, p < 0.001;
458 **, p < 0.01; *, p < 0.05; n.s. (not significant), p > 0.05). ND: not detected.
459

460 **Figure 4.** 2'-O-MTase mutant viruses induce nuclear localization of IRF3 in WT, but not
461 MDA5-deficient M Φ s. **a)** Detection of IRF3 in MHV-A59, MHV-Y15A or MHV-D130A
462 infected (MOI=1) murine M Φ s derived from *ifnar*^{-/-} (upper row) or *mda5*^{-/-} (lower row) mice.
463 Cells were stained at 3 h p.i. for IRF3 (red) and DAPI (blue). Representative fields are shown. **b)**
464 The percentage of cells with IRF3 located in the nucleus was calculated for each

465 immunofluorescence analysis using five random fields with approximately 50-250 cells each.
466 Results represent the mean \pm SD. Statistical analysis was done using unpaired Student's t-test
467 (***, p < 0.001; **, p < 0.01; *, p < 0.05; n.s. (not significant), p > 0.05). ND: not detected.

468

469 **Figure 5.** MDA5 is critical for replication restriction of the IFN-I sensitive MHV 2'-O-
470 MTase active site mutant MHV-D130A but not for the MHV-Y15A mutant. **a-b)** Murine MΦs
471 (1×10^6) derived from WT (left panels) or MDA5^{-/-} (right panels) mice were infected with MHV-
472 A59, MHV-D130A or MHV-Y15A at an MOI=1 (**a**) or MOI=0.0001 (**b**). Viral titers in the cell
473 culture supernatants were measured at the indicated time points by plaque assay. Results
474 represent the mean \pm SEM of two independent experiments (n=5). **c-d)** IFN-sensitivity of MHV
475 2'-O-MTase mutants. Murine MΦs (1×10^5) derived from WT (**c**) or
476 MDA5^{-/-} (**d**) mice were treated with the indicated dosages of IFN- α for 4 h prior to infection
477 (MOI=1) with MHV-A59, MHV-D130A or MHV-Y15A. Viral titers in the cell culture
478 supernatants were measured at 24 h p.i.. Results represent the mean \pm SD of two independent
479 experiments (n=4).

480

481 **Figure 6.** MHV replication kinetics in *ifit1*^{-/-} MΦs. **a,b)** Murine MΦs (5×10^5) derived from
482 WT (**a**) or *ifit1*^{-/-} (**b**) mice were infected with MHV-WT, MHV-D130A, or MHV-Y15A at and
483 MOI of 0.01. Viral titers in the cell culture supernatants were measured at the indicated time
484 points by plaque assay. Results represent the mean \pm SEM of two independent experiments (n=4).

485

486 **Figure 7.** MHV 2'O-MTase mutants are highly attenuated in WT mice but restore
487 efficient replication in *ifnar*^{-/-} and *mda5*^{-/-}/*tlr7*^{-/-} mice. WT, *ifnar*^{-/-}, *mda5*^{-/-}/*tlr7*^{-/-}, *mda5*^{-/-}, and
488 *tlr7*^{-/-} mice (6-8 week old) were infected intraperitoneally with 500 p.f.u of MHV-A59, MHV-

489 D130A or MHV-Y15A. Viral titers in spleens (**a**) and livers (**b**) were determined at 24 h p.i.
490 Results represent the mean \pm SD of two independent experiments (n=6). ND: not detected.

491

492 **ACKNOWLEDGEMENTS**

493 This work was supported by the Swiss National Science Foundation, the Novartis
494 Foundation for Biomedical Research, Switzerland, the German Ministry of Education and
495 Research (to V.T.), the Austrian Science Fund (to M.H.), the Deutsche Forschungsgemeinschaft
496 (to J.Z.), the National Institutes of Health, USA (AI060915 and AI085089 to S.C.B.; U54
497 AI081680 [Pacific Northwest Regional Center of Excellence for Biodefense and Emerging
498 Infectious Diseases Research] to M.S.D), the Medical Research Council Capacity Building
499 Studentship (to B.W.N.), and the Wellcome Trust (to S.G.S.). The authors are indebted to Lucas
500 Onder for assistance in fluorescence microscopy, and to Rita de Giuli, Barbara Schelle, and
501 Nadja Karl for excellent technical assistance.

502

503 **AUTHOR CONTRIBUTIONS**

504 R.Z., L.C-B, M.H., R.M., and K.J.S. did most of the experiments. B.W.N. did phylogenetic
505 analyses. B.W.N. and S.C.B. did electron microscopy. J.Z., S.C.B., W.B., M.S.D., S.G.S., and
506 B.L. contributed key research reagents and expertise. S.G.S., B.W.N., B.L., and V.T. conceived
507 and designed the project and wrote and edited the manuscript.

508

509 **REFERENCES**

510 1. Janeway, C. A., Jr. Approaching the asymptote? Evolution and revolution in
511 immunology. *Cold Spring Harb Symp Quant Biol* **54 Pt 1**, 1-13 (1989).

512 2. Takeuchi, O. & Akira, S. Innate immunity to virus infection. *Immunol Rev* **227**, 75-86
513 (2009).

514 3. Loo, Y. M. & Gale, M., Jr. Viral regulation and evasion of the host response. *Curr Top*
515 *Microbiol Immunol* **316**, 295-313 (2007).

516 4. Haller, O. & Weber, F. Pathogenic viruses: smart manipulators of the interferon system.
517 *Curr Top Microbiol Immunol* **316**, 315-34 (2007).

518 5. Hui, D. J., Terenzi, F., Merrick, W. C. & Sen, G. C. Mouse p56 blocks a distinct function
519 of eukaryotic initiation factor 3 in translation initiation. *J Biol Chem* **280**, 3433-40
520 (2005).

521 6. Terenzi, F., Hui, D. J., Merrick, W. C. & Sen, G. C. Distinct induction patterns and
522 functions of two closely related interferon-inducible human genes, ISG54 and ISG56. *J*
523 *Biol Chem* **281**, 34064-71 (2006).

524 7. Fensterl, V. & Sen, G. C. The ISG56/IFIT1 Gene Family. *J Interferon Cytokine Res*.

525 8. Kato, H. et al. Length-dependent recognition of double-stranded ribonucleic acids by
526 retinoic acid-inducible gene-I and melanoma differentiation-associated gene 5. *J Exp*
527 *Med* **205**, 1601-10 (2008).

528 9. Hornung, V. et al. 5'-Triphosphate RNA Is the Ligand for RIG-I. *Science* **314**, 994-7
529 (2006).

530 10. Pichlmair, A. et al. RIG-I-mediated antiviral responses to single-stranded RNA bearing
531 5'-phosphates. *Science* **314**, 997-1001 (2006).

532 11. Schlee, M. et al. Recognition of 5' triphosphate by RIG-I helicase requires short blunt
533 double-stranded RNA as contained in panhandle of negative-strand virus. *Immunity* **31**,
534 25-34 (2009).

535 12. Ghosh, A. & Lima, C. D. Enzymology of RNA cap synthesis. *Wiley Interdisciplinary*
536 *Reviews: RNA* **1**, 152-172 (2010).

537 13. Shuman, S. What messenger RNA capping tells us about eukaryotic evolution. *Nat Rev*
538 *Mol Cell Biol* **3**, 619-25 (2002).

539 14. Nomoto, A., Detjen, B., Pozzatti, R. & Wimmer, E. The location of the polio genome
540 protein in viral RNAs and its implication for RNA synthesis. *Nature* **268**, 208-13 (1977).

541 15. Hemmi, H. et al. A Toll-like receptor recognizes bacterial DNA. *Nature* **408**, 740-5
542 (2000).

543 16. Bouvet, M. et al. In vitro reconstitution of SARS-coronavirus mRNA cap methylation.
544 *PLoS Pathog* **6**, e1000863 (2010).

545 17. Chen, Y. et al. Functional screen reveals SARS coronavirus nonstructural protein nsp14
546 as a novel cap N7 methyltransferase. *Proc Natl Acad Sci U S A* **106**, 3484-9 (2009).

547 18. Decroly, E. et al. Coronavirus nonstructural protein 16 is a cap-0 binding enzyme
548 possessing (nucleoside-2'O)-methyltransferase activity. *J Virol* **82**, 8071-84 (2008).

549 19. Snijder, E. J. et al. Unique and conserved features of genome and proteome of SARS-
550 coronavirus, an early split-off from the coronavirus group 2 lineage. *J Mol Biol* **331**, 991-
551 1004 (2003).

552 20. Schnierle, B. S., Gershon, P. D. & Moss, B. Cap-specific mRNA (nucleoside-O2'-)-
553 methyltransferase and poly(A) polymerase stimulatory activities of vaccinia virus are
554 mediated by a single protein. *Proc Natl Acad Sci U S A* **89**, 2897-901 (1992).

555 21. Cervantes-Barragan, L. et al. Type I IFN-mediated protection of macrophages and
556 dendritic cells secures control of murine coronavirus infection. *J Immunol* **182**, 1099-106
557 (2009).

558 22. Cervantes-Barragan, L. et al. Control of coronavirus infection through plasmacytoid
559 dendritic-cell-derived type I interferon. *Blood* **109**, 1131-7 (2007).

560 23. Rose, K. M., Elliott, R., Martinez-Sobrido, L., Garcia-Sastre, A. & Weiss, S. R. Murine
561 coronavirus delays expression of a subset of interferon-stimulated genes. *J Virol* **84**,
562 5656-69.

563 24. Roth-Cross, J. K., Bender, S. J. & Weiss, S. R. Murine coronavirus mouse hepatitis virus
564 is recognized by MDA5 and induces type I interferon in brain macrophages/microglia. *J
565 Virol* **82**, 9829-38 (2008).

566 25. Zhou, H., Zhao, J. & Perlman, S. Autocrine interferon priming in macrophages but not
567 dendritic cells results in enhanced cytokine and chemokine production after coronavirus
568 infection. *MBio* **1** (2010).

569 26. Bocharov, G. et al. A Systems Immunology Approach to Plasmacytoid Dendritic Cell
570 Function in Cytopathic Virus Infections. *PLoS Pathog* (in press).

571 27. Daffis, S. et al. 2'-O methylation of the viral mRNA cap evades host restriction by IFIT
572 family members. *Nature* **468**, 452-456 (2010).

573 28. Thiel, V. & Weber, F. Interferon and cytokine responses to SARS-coronavirus infection.
574 *Cytokine Growth Factor Rev* **19**, 121-32 (2008).

575 29. Loo, Y. M. et al. Distinct RIG-I and MDA5 signaling by RNA viruses in innate
576 immunity. *J Virol* **82**, 335-45 (2008).

577 30. Morin, B. et al. The N-terminal domain of the arenavirus L protein is an RNA
578 endonuclease essential in mRNA transcription. *PLoS Pathog* **6** (2010).

579 31. Reguera, J., Weber, F. & Cusack, S. Bunyaviridae RNA polymerases (L-protein) have an
580 N-terminal, influenza-like endonuclease domain, essential for viral cap-dependent
581 transcription. *PLoS Pathog* **6** (2010).

582 32. Qi, X. et al. Cap binding and immune evasion revealed by Lassa nucleoprotein structure.
583 *Nature* (2010).

584 33. Le Gall, O. et al. Picornavirales, a proposed order of positive-sense single-stranded RNA
585 viruses with a pseudo-T = 3 virion architecture. *Arch Virol* **153**, 715-27 (2008).

586 34. Gitlin, L. et al. Essential role of mda-5 in type I IFN responses to
587 polyriboinosinic:polyribocytidylc acid and encephalomyocarditis picornavirus. *Proc
588 Natl Acad Sci U S A* **103**, 8459-64 (2006).

589 35. Nallagatla, S. R. & Bevilacqua, P. C. Nucleoside modifications modulate activation of
590 the protein kinase PKR in an RNA structure-specific manner. *Rna* **14**, 1201-13 (2008).

591 36. Kariko, K., Buckstein, M., Ni, H. & Weissman, D. Suppression of RNA recognition by
592 Toll-like receptors: the impact of nucleoside modification and the evolutionary origin of
593 RNA. *Immunity* **23**, 165-75 (2005).

594 37. Nallagatla, S. R., Toroney, R. & Bevilacqua, P. C. A brilliant disguise for self RNA: 5'-
595 end and internal modifications of primary transcripts suppress elements of innate
596 immunity. *RNA Biol* **5**, 140-4 (2008).

597 38. Eriksson, K. K., Makia, D. & Thiel, V. Generation of recombinant coronaviruses using
598 vaccinia virus as the cloning vector and stable cell lines containing coronaviral replicon
599 RNAs. *Methods Mol Biol* **454**, 237-54 (2008).

600 39. Zust, R. et al. Coronavirus non-structural protein 1 is a major pathogenicity factor:
601 implications for the rational design of coronavirus vaccines. *PLoS Pathog* **3**, e109 (2007).

602 40. Wunschmann, S., Becker, B. & Vallbracht, A. Hepatitis A virus suppresses monocyte-to-
603 macrophage maturation in vitro. *J Virol* **76**, 4350-6 (2002).

604 41. Uze, G. et al. Domains of interaction between alpha interferon and its receptor
605 components. *J Mol Biol* **243**, 245-57 (1994).

606 42. Fauman, E. B., Blumenthal, R. M. & Chemg, X. in *S-Adenosylmethionine-Dependent*
607 *Methyltransferases: Structures and Functions* (eds. Cheng, X. & Blumenthal, R. M.) 1-
608 38 (World Scientific, Singapore, 1999).

609 43. Feder, M., Pas, J., Wyrwicz, L. S. & Bujnicki, J. M. Molecular phylogenetics of the
610 RrmJ/fibrillarin superfamily of ribose 2'-O-methyltransferases. *Gene* **302**, 129-38 (2003).

611 44. Larkin, M. A. et al. Clustal W and Clustal X version 2.0. *Bioinformatics* **23**, 2947-8
612 (2007).

613 45. Bryson, K. et al. Protein structure prediction servers at University College London.
614 *Nucleic Acids Res* **33**, W36-8 (2005).

615 46. Waterhouse, A. M., Procter, J. B., Martin, D. M., Clamp, M. & Barton, G. J. Jalview
616 Version 2--a multiple sequence alignment editor and analysis workbench. *Bioinformatics*
617 **25**, 1189-91 (2009).

618

619

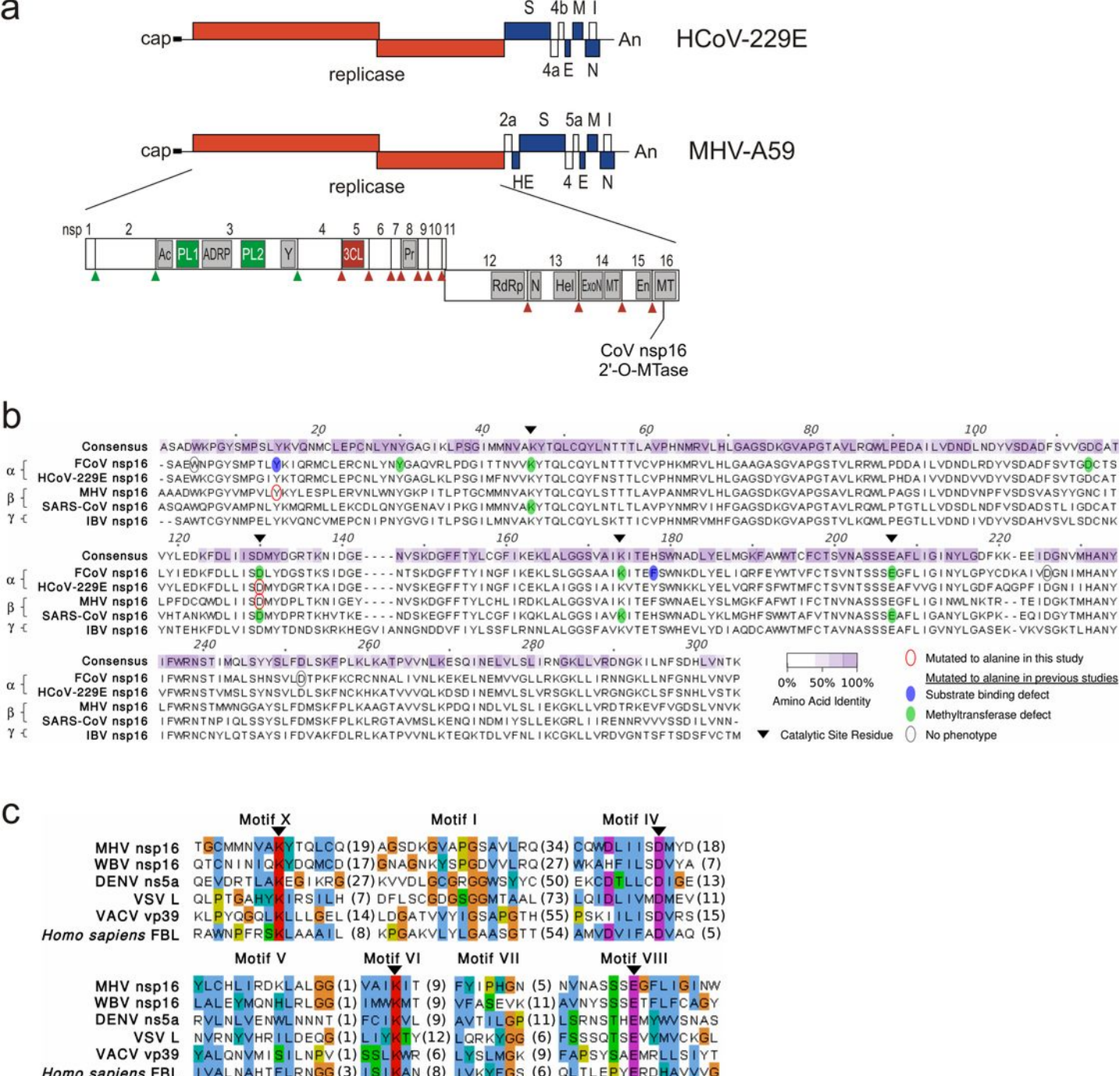


Figure 1

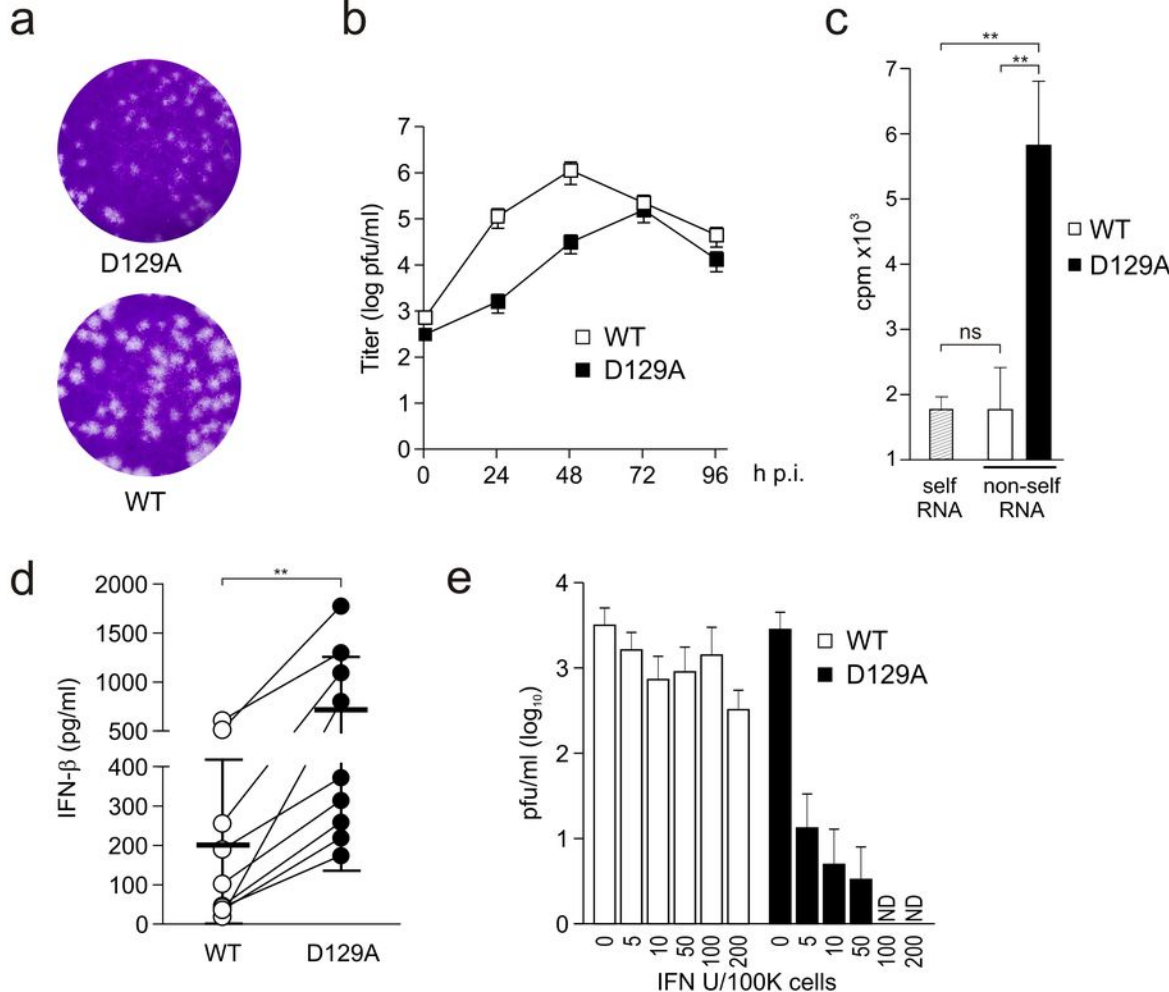


Figure 2

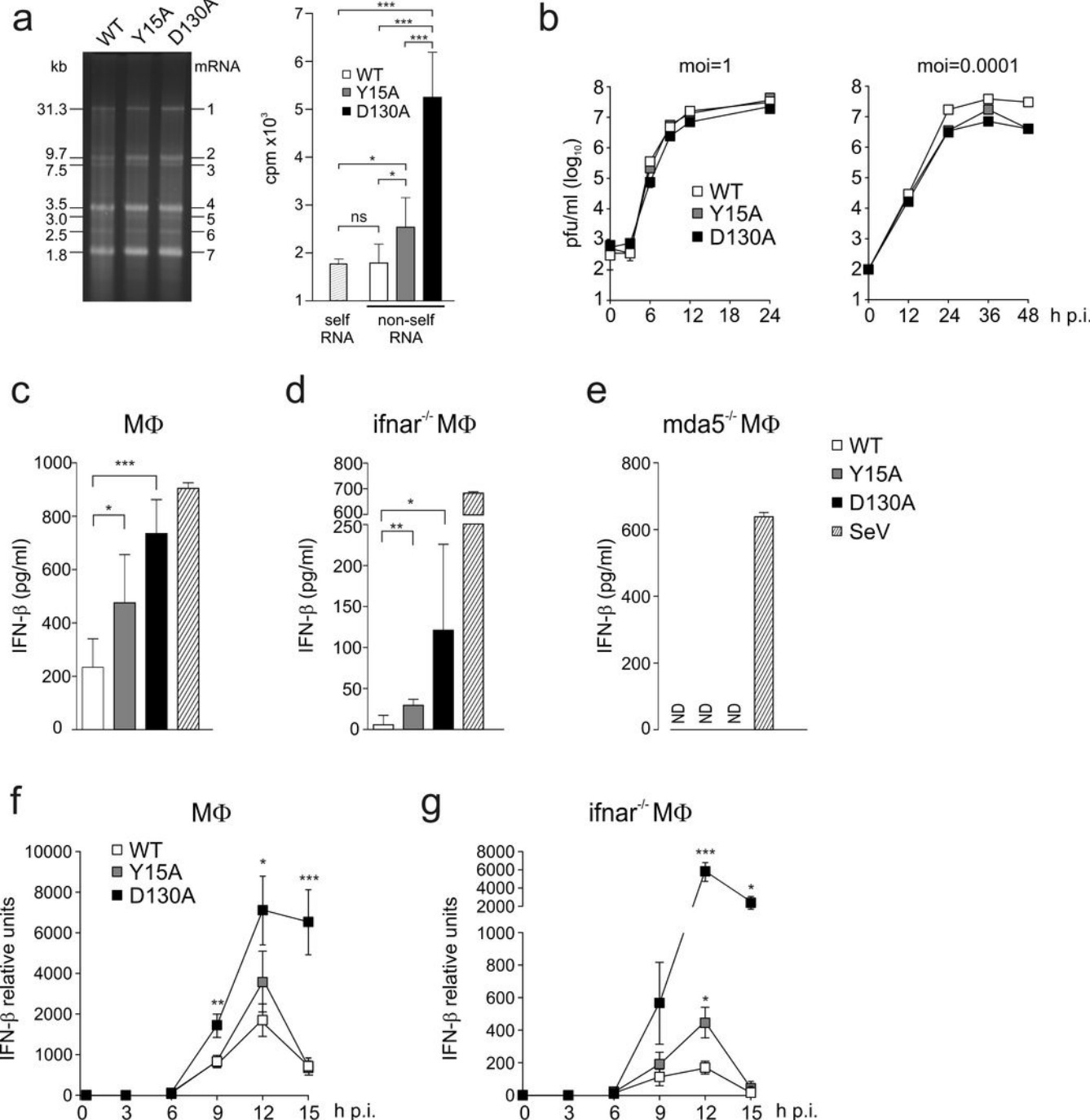
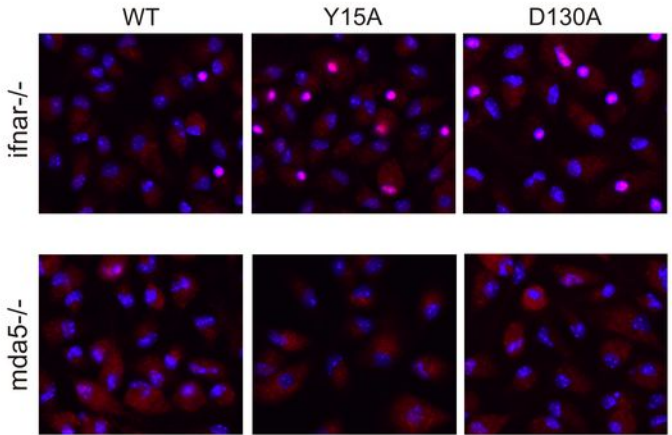
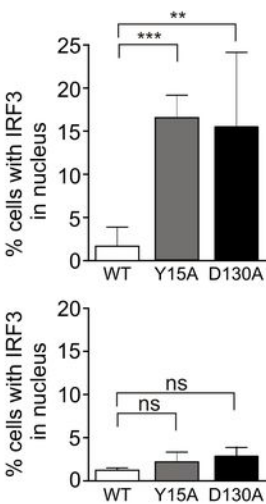


Figure 3

a**b****Figure 4**

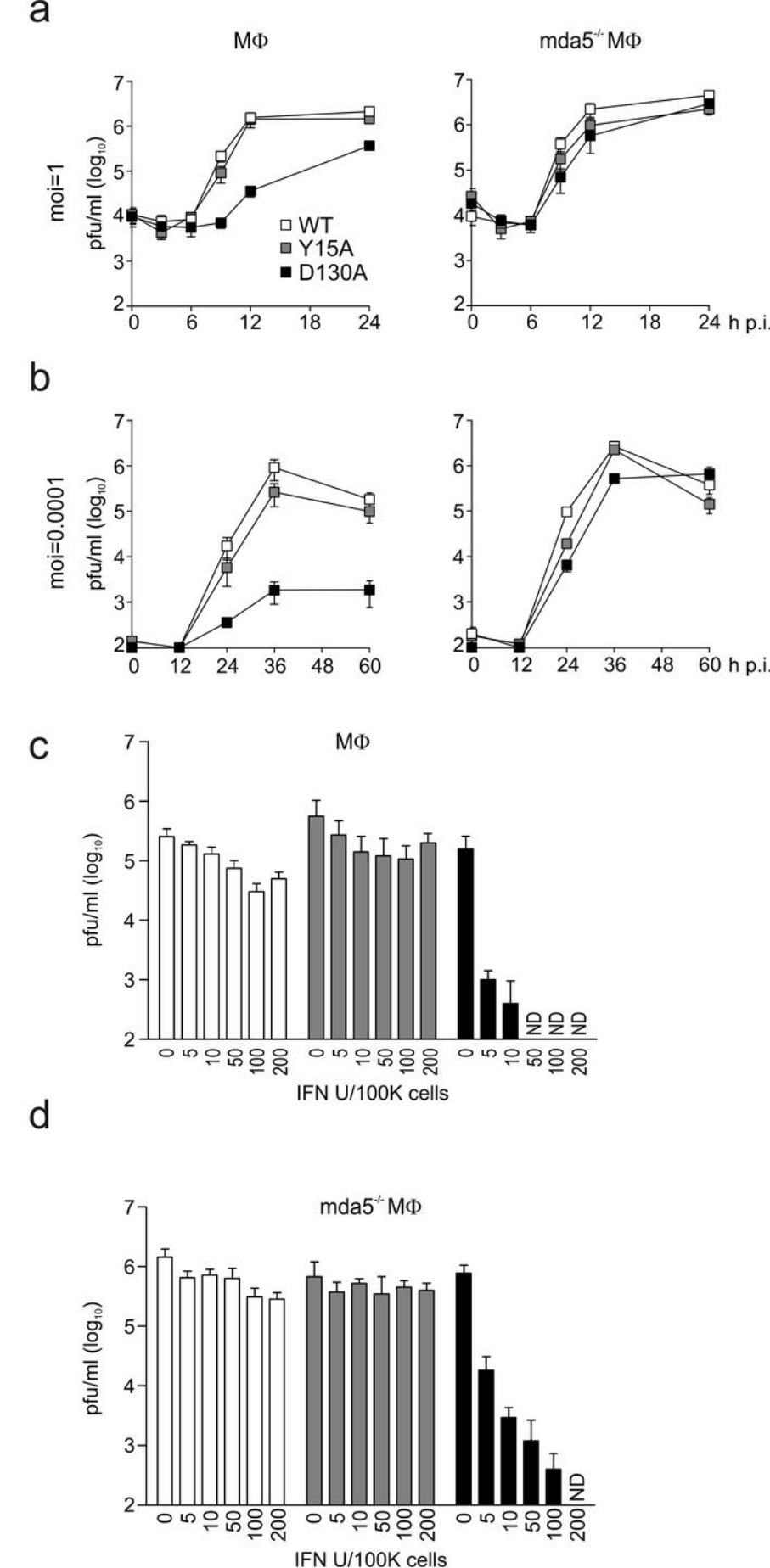


Figure 5

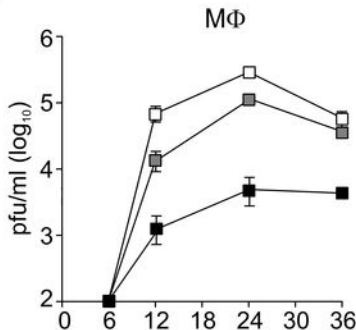
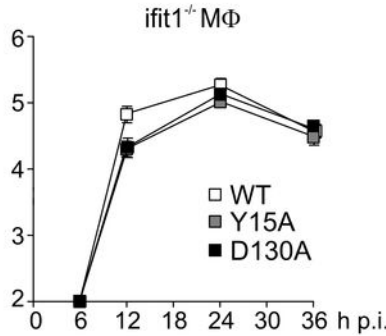
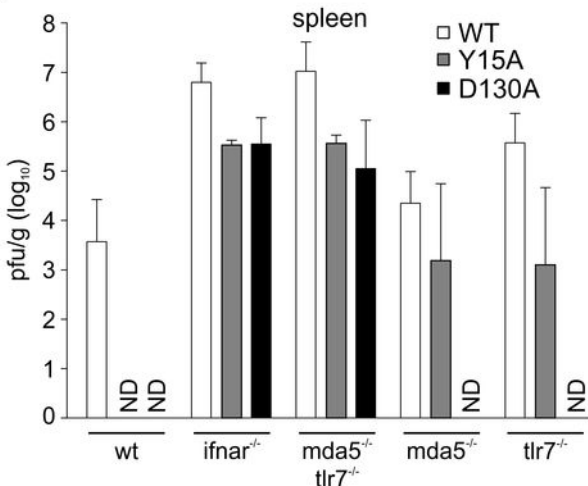
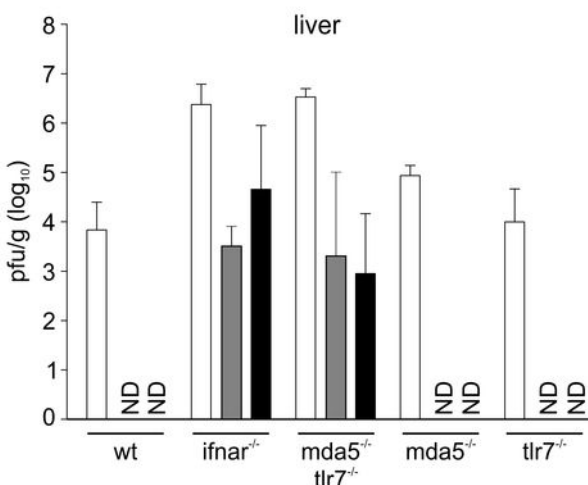
a**b**

Figure 6

a**b****Figure 7**